# Characterization of Laser Driven Shocks in Low Density Foam Targets

D. Hoarty,[1,2] A. Iwase,[1] C. Meyer,[1] J. Edwards,[2] and O. Willi[1]
[1]*The Blackett Laboratory, Imperial College of Science, Technology and Medicine, London, SW7 2BZ, United Kingdom*
[2]*Radiation Physics Department, AWE Aldermaston, Reading, Berkshire, RG7 4PR, United Kingdom*
(Received 5 June 1996)

Laser driven shock waves propagating through foam targets have been diagnosed by side-on time-resolved x-ray absorption spectroscopy. *K*-shell absorption spectra of chlorine, doped into the foam targets, were matched to a detailed atomic physics model to infer the temperature profile. The density distribution was obtained from the x-ray transmission through the target. 2D radiation-hydrodynamic modeling of the targets reproduced the experimental results. Preheating of material by radiation from the shocked region was shown to have an important contribution to the measured temperature profile. [S0031-9007(97)02993-1]

PACS numbers: 52.50.Jm, 52.25.Nr

Shock wave studies have investigated a wide variety of phenomena, including energy transfer, chemical reaction rates, and the equation of state of material at high density and pressure [1,2]. Experimental studies have been pursued for many years in shock tubes driven by explosives and magnetic fields, in strong explosions in gases [1], as well as more recently in laser irradiated targets [3]. With the development of foam technology there is now an opportunity to access a density regime in between those studied previously in solids and gases. The low specific heat of foams results in high shock temperatures being readily achieved, and their low density allows x rays to penetrate the foam which is useful for both diagnostic probing and studying radiation associated with the shock. Radiative phenomena associated with shocks have been shown to be important in a variety of astrophysical flows [4] and are crucial to the understanding and achievement of inertial confinement fusion [5].

In order to characterize a shock wave in a material, at least two parameters must be measured simultaneously [1]. Many experiments have concentrated on measuring shock velocity, which is relatively easy to measure, and the fluid velocity behind the shock. The thermodynamic properties, for example, the density and temperature, are then derived. Direct measurements of the thermodynamic properties have proved difficult. For example, shock temperatures inferred from optical pyrometry in solid targets have required detailed hydrodynamic simulations to interpret the data due to the release of the target surface immediately upon shock breakout [1]. Such simulations can be in error due to uncertainties in opacity, equation of state data, and in radiation transport. There are also errors in the measurements arising from thermal equilibration and gradients [6]. Shock temperature measurements in gaseous targets have used emission spectroscopy and line reversal techniques which suffer from errors due to nonequilibrium and opacity effects [2,7]. Several workers have used foam targets to study shock propagation, using radiography to track the shock front or infer the density [8]. This Letter reports the first simultaneous measurement of the density and temperature distribution in a strongly shocked material via a novel application of x-ray absorption spectroscopy. The shock, driven by laser ablation, propagated through a foam target and was diagnosed using short pulse x-ray absorption spectroscopy, viewing side-on to the shock propagation. The density profile was obtained from the absolute transmission and the temperature profile inferred from the absorption spectrum of chlorine ions chemically doped into the target. The measured shock position allowed the shock velocity to be inferred. The measurements showed the effect of the preheating of material ahead of the front by radiation from the shock. Simulated profiles from 2D radiation hydrodynamics calculations reproduced the measured profiles.

The experiments used cylindrical triacrylate foam targets at a density of 50 $mg/cm^3$ which were doped with chlorinated triacrylate ($C_9H_3O_2Cl_5$) to give a concentration of 25% by weight of chlorine [9]. The initial foam density and chlorine content were measured by radiography. The foams had a high degree of homogeneity with an average pore size diameter of 1 $\mu$m and were typically between 170 and 200 $\mu$m long and between 200–300 $\mu$m in diameter. Two frequency doubled beams (wavelength $\sim$0.53 $\mu$m) of the VULCAN laser system were focused with $f/10$ lenses onto one end of the cylindrical target, producing an irradiance of $1 \times 10^{14}$ $W/cm^2$ in a pulse of 700 ps width (FWHM) with a rise time of 400 ps. The spatial profile of the laser spot was approximately Gaussian and fell off by 70% from the center to the edge of the foam cylinder. Phase plates were used to smooth the laser beams. Previous work [10] has shown that small scale laser nonuniformities are smoothed in foam targets due to lateral electron conduction. The induced shock was observed perpendicularly to the axis of the cylindrical target. The effect of nonuniformity in the beam focusing on the planarity of the shock could be observed in the radiographs, and the data were rejected if the shock planarity was compromised. The shocked foam was radiographed by a point source of x rays from a combination bismuth/

 0031-9007/97/78(17)/3322(4)$10.00 

gold backlighter pin irradiated with a 0.53 $\mu$m wavelength laser beam, of 70 ps pulse length, focused with a $f/2.5$ lens. The radiographs were recorded using a flat crystal spectrometer with a thallium acid phthalate crystal ($2d$ spacing 25.75 Å, spectral resolution 5 eV) and x-ray film. The spectral range of the spectrometer was set to record the absorption spectrum of chlorine due to transitions from the $K$ shell to the $2p$ and $3p$ orbitals (2.5–3.0 keV). The spectrometer was aligned to record the x rays passing through and around the foam, allowing the absolute transmission of the foam to be obtained. Absorption spectra were recorded at different times in the transit of the shock through the foam by varying the delay of the backlighting beam relative to the beams irradiating the foam. Data were recorded at 350 ps after the start of the pulse, and at 850 ps after the start (the start of the pulse being 400 ps before the peak). The time resolution was determined by the pulse length of the backlighter laser beam because the duration of emission at 2.5–3.0 keV from the backlighter pin closely follows the laser pulse. The spatial resolution was determined by radiographing alignment disks and pinholes, and was found to be 8 $\mu$m in the direction of shock propagation. The shock velocity was deduced from the position of the shock front in the target and from separate shots with a streaked extreme ultraviolet (XUV) imaging system. An x-ray diode monitored the time resolved, frequency integrated emission from the foam and the backlighter pin on every shot. Optical diagnostics measured the shape of the laser pulse and energy. Figure 1 shows a schematic diagram of the experimental arrangement.

The chlorine $K$-shell absorption spectra were compared to a model of the population of chlorine charge configurations which assumed local thermodynamic equilibrium (LTE). The material density was obtained from the measured continuum transmission (see below) and input to the model. Saha-Boltzmann statistics were used to calculate the relative populations in configurations of the chlorine charge states with a full $K$ shell, including all permutations of $L$-shell electrons, satellites in $M$ and $N$ shells, and detailed term structure. A detailed spectrum was then constructed, using transition energies and oscillator strengths from *ab initio* calculations by the multiconfiguration Dirac-Fock code GRASP [11]. $K$ edge energies and cross sections were calculated from parametric fits [12]. The model included the continuum lowering treatment of Stewart and Pyatt [13]. A Gaussian instrument resolution function was used in the simulated spectra. The contribution to the continuum opacity and the contribution to the electron density from the other constituents of the foam were included. To infer temperature, the model temperature was iterated until the best agreement between the experimental and calculated spectra was obtained at the measured density. Temporal and spatial gradients were taken into account by a weighted sum of the contribution of calculational cells at different temperatures and densities.

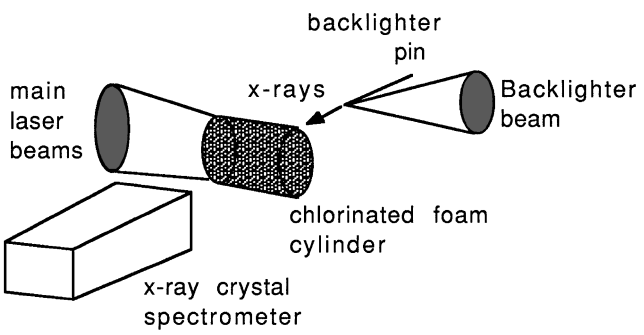


FIG. 1. The experimental arrangement for point projection radiography of the foam.

The LTE assumption was checked by performing collisional radiative calculations using a model based on the GALAXY code [14] with improved energy levels and continuum lowering [13]. At each data point the ionization was calculated using LTE and non-LTE modeling, with the radiation temperature input $T_r$ taken from the radiation hydrodynamics simulations (see below). It was found that the ionization did not depart from the LTE value by more than 1% in the shocked region or even in the radiatively preheated region immediately ahead of the shock front where the difference between $T_r$ and $T_e$ was large (30–35 eV). The electron density of the foam, $2.5 \times 10^{22}/\mathrm{cm}^3$ in the peak of the shock falling to $8 \times 10^{21}/\mathrm{cm}^3$ immediately ahead of the shock front, was such that, for the configurations considered, populations were dominated by collisional processes giving an ionization characteristic of the electron temperature $T_e$. These calculations assumed steady state, which was a valid assumption because the collisional radiative rates (approximately 1 ps) are much faster than the time scale of changes in the shock parameters.

One- and two-dimensional Lagrangian radiation hydrodynamics simulations of the foam targets were performed using the NYM code [15]. The code included inverse bremsstrahlung and resonance laser absorption; flux limited thermal conduction with a flux limiter of 0.05, multigroup opacities calculated from the IMP code [16], radiation transport using the Implicit Monte Carlo formalism [17], and tabulated equation of state data. The foam was treated as a continuous medium of uniform density. The simulations predicted preheat of 2 eV, which would have the effect of closing the pores of the foam before the shock arrived. The pore closure time was estimated to be around 200 ps after the start of the laser pulse. The assumption of a shock passing through a continuous medium was therefore expected to be valid.

A radiograph is shown in Fig. 2, divided into four areas illustrating the unattenuated backlighter signal (1), the transmission through the unshocked foam (2), the shocked region showing the absorption features characteristic of ionized chlorine (3), and the rarefraction behind the laser ablation surface (4). The rear of the foam is clearly visible, allowing the shock position to be measured accurately. Side-on XUV imaging showed that the rear of the

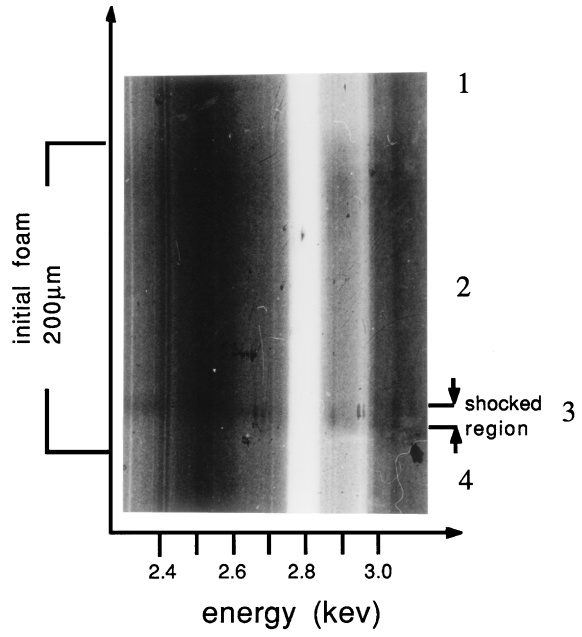


FIG. 2. A radiograph of the foam target at $t = +350$ ps.

foam did not change position until well after the profile measurements were taken. A scan through the unshocked foam allowed the chlorine content and initial density to be verified by comparison of the transmission at frequencies above and below the cold chlorine $K$ edge frequency.

The density of the shocked region was obtained by comparing the continuum transmission in the shocked and unshocked material at the same frequency [8] (away from the chlorine $K$-shell lines and the absorption edge). The continuum opacity softer than the chlorine $K$ lines (between 2.4 and 2.5 keV) changes little between cold and heated foam, and the slight difference can be neglected. A plot of the density profile is shown in Fig. 3 compared to the 2D simulation. The 2D simulation was convolved by the spatial resolution and shifted $-5$ $\mu$m to coincide with the experimental data points. The position of experimental data at the front of the density profile was shifted by $-4$ $\mu$m to account for the shock movement during the backlighter pulse based on the measured shock velocity and backlighter pulse duration. The errors in the measured density come from limitations in temporal and spatial resolution. The temperature profile of the shocked material was obtained as described above at the measured density. The He-like chlorine $1s2p$-$1s^2$ emission masked some of the spectrum in line scans close to the ablation surface, but charge states observed in the shock region were soft enough not to be obscured. The $n = 1$ to $n = 2$ absorption in the shock region was typically in F-like to C-like ions. Figure 4(a) shows the transmission through the shocked region plotted against frequency at 350 ps after the start of the pulse. The $n = 1$ to $n = 2$ absorption features can be clearly seen. At this time, the laser is nearing peak irradiance. Overplotted is the simulated spectrum (dashed line) as an example of the fit

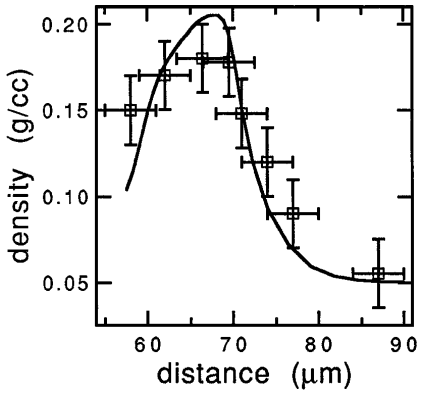


FIG. 3. The density profile through the shocked region at $+850$ ps compared to simulation prediction. The squares are the experimental points; the solid line is the simulation.

to the experimental data. Figure 4(b) shows the spectrum and fit at $+850$ ps, offset for clarity. The temperatures inferred from fits to the absorption spectra are accurate to within $\pm 3$ eV over the range of temperatures from 35–65 eV. Density changes $> \times 2$ are required to change the observed spectrum by more than the effect of a 3 eV temperature change. Since lines in the most abundant ions of the distribution were optically thick, it was the transmission in less populated ions that gave the sensitivity to changes in temperature. The model showed that the sensitivity to temperature decreased below 35 eV because only a single $n = 1$ to $n = 2$ feature from F-like chlorine and lower charge states was present. This feature disappeared below 22 eV. Lower temperatures were obtained from the remaining $n = 1$ to $n = 3$ absorption with less accuracy.

Shock movement during the backlighter pulse was calculated from the known backlighter duration and the measured shock velocity. A shock width of 8 $\mu$m was inferred from the observed width at a backlighter delay of 350 ps. This was the spatial resolution limit of the backlighter and so implied an upper limit to the shock width at $+350$ ps. Although the

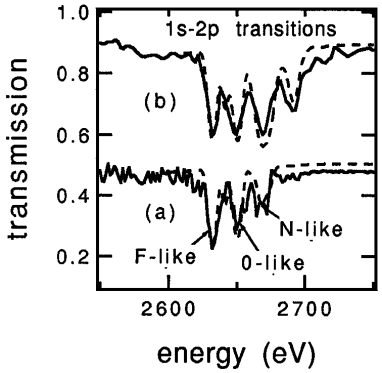


FIG. 4. An example of the fit between an experimental absorption spectrum and the spectral simulation (dashed) at 350 ps ($a$) and 850 ps ($b$). Curve ($b$) is offset by $+0.4$ for clarity.

shocked region was too narrow to measure the shock front temperature profile at +350 ps, the temperature behind the front was obtained. The inferred temperature was 49 eV; 48 eV was predicted by the 2D simulation. At 850 ps the shock width had increased several times, reducing the spatial resolution problems significantly. For the data with a time delay of 850 ps the spatial temperature profile of the shocked region was obtained from line outs at various positions measured from the rear of the foam in the radiograph. The temperature in the shocked region was found to rise sharply then level off before increasing rapidly close to the ablation surface. Good fits of the model spectrum and the experimental data were obtained in the plateau region with a single temperature. At the steep falloff ahead of the plateau a composite of more than one temperature was required to obtain agreement between the model and the experimental spectra. This is not surprising and is caused by the movement of the shock during the backlighter pulse. The time scale on which the shock parameters changed was greater than the backlighter duration. The movement was small compared with the total width of the shocked region, and part of the isothermal region behind the shock front showed no temporal blurring in the data. Knowledge of the shock velocity and backlighter duration allowed the shape of the moving step profile to be unfolded. The inferred instantaneous temperature profile is shown in Fig. 5. The measurements were compared to predictions of the radiation hydrodynamics code. The simulation result convolved with the 8 $\mu$m spatial resolution is also shown in Fig. 5. In addition, a spatial shift between 3 and 5 $\mu$m for different shots was required at nominally the same delay and irradiance. This corresponds to an uncertainty in the relative timing of the heating beam and the backlighter of up to 50 ps. This is consistent with the accuracy of the relative timing as the heating and backlighter pulses were generated from different oscillators. Estimates of the extent of shock curvature were made from comparing 1D and 2D calculations for Gaussian beam profiles. Differences in position and temperature were small, but the 2D calculation was in better agreement with the experimentally measured width of the shocked region. The radiation hydrodynamics code was run also for a case where no radiation came from the shocked region. In this case, the foot of the temperature profile at temperatures below 20 eV, which can be seen in Fig. 5, was greatly reduced, showing that the foot was predominantly due to heating by radiation from the shocked material.

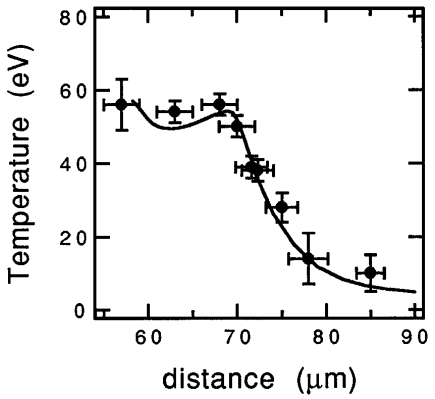


FIG. 5. The shock temperature profile at $t = +850$ ps compared to simulation prediction. The dots with error bars are the experimental points; the solid line is the simulation.

In summary, for the first time, detailed, simultaneous measurements have been made of the temperature and density profiles in radiating shock waves through a novel application of absorption spectroscopy. The temperature in the shocked region was inferred from LTE modeling of the absorption spectra of chlorine, doped into foam targets, twice during the shock propagation. The density was inferred directly from the target transmission. The validity of the LTE modeling was checked by detailed collisional-radiative calculations of the experimental conditions including the effect of radiation. The inferred profiles and shock velocities were compared to 2D radiation hydrodynamics simulations convoluted with the experimental spatial resolution, and were in good agreement.

This work was partly supported by EPSRC/MoD grants. We would like to thank the staff of the VULCAN laser and Dr. C. C. Smith for help in compiling the atomic physics database and for many useful discussions, and G. Lyall, J. Falconer, and W. Nazarov (Dundee University) for supplying the foam targets.

[1] Ya. B. Zel'dovich and Yu. P. Raizer, *Physics of Shock Waves and High Temperature Hydrodynamic Phenomena* (Academic, New York, 1966).
[2] J. N. Bradley, *Shock Waves in Chemistry and Physics* (Wiley, New York, 1962).
[3] F. Cottet *et al.,* Phys. Rev. Lett. **52**, 1884 (1984).
[4] D. Mihalas, *Foundations of Radiation Hydrodynamics* (Oxford University Press, New York, 1984).
[5] J. Lindl, Phys. Plasmas **2**, 3933 (1995).
[6] P. Celliers, A. Ng, G. Xu, and A. Forsman, Phys. Rev. Lett. **68**, 2305 (1992).
[7] R. I. Soloukin, *Shock Waves and Detonations in Gases* (Mono Book Corp., Baltimore, 1966).
[8] B. A. Hammel *et al.,* Phys. Fluids B **5**, 2259 (1993).
[9] J. W. Falconer *et al.,* J. Vac. Sci. Technol. A **8**, (2), 968 (1990).
[10] M. Dunne *et al.,* Phys. Rev. Lett. **75**, 3858 (1995).
[11] K. G. Dyall *et al.,* Comput. Phys. Commun. **55**, 425 (1989).
[12] R. E. H. Clark *et al.,* At. Data Nucl. Data Tables **34**, 415 (1986).
[13] J. Stewart and K. Pyatt, Astrophys. J. **144**, 1203 (1966).
[14] S. J. Rose, J. Quant. Spectrosc. Radiat. Transf. **54**, 333 (1995).
[15] P. D. Roberts, AWE report, 1980 (unpublished).
[16] S. J. Rose, J. Phys. B **25**, 1667 (1992).
[17] J. A. Fleck and J. D. Cummings, J. Comput. Phys. **8**, 313 (1971).